

# In-situ observation for RH-dependent mixing states of submicron particles containing organic surfactants and inorganic salts

Chun Xiong<sup>1#</sup>, Binyu Kuang<sup>1#</sup>, Fei Zhang<sup>1</sup>, Xiangyu Pei<sup>1</sup>, Zhengning Xu<sup>1</sup>, Zhibin Wang<sup>1,2,3\*</sup>

<sup>1</sup>College of Environmental and Resource Sciences, Zhejiang University, Zhejiang Provincial Key Laboratory of Organic Pollution Process and Control, Hangzhou, 310058, China

<sup>2</sup>ZJU-Hangzhou Global Scientific and Technological Innovation Center, Zhejiang University, Hangzhou 311215, China

<sup>3</sup>Key Laboratory of Environment Remediation and Ecological Health, Ministry of Education, Zhejiang University, Hangzhou, 310058, China

\*Correspondence to Zhibin Wang ([wangzhibin@zju.edu.cn](mailto:wangzhibin@zju.edu.cn))

# Chun Xiong and Binyu Kuang contribute equally to this work.

**Abstract:** Aerosol mixing state plays an important role in heterogeneous reactions and CCN activity. Organic surfactants could affect aerosol mixing state through bulk-surface partitioning. However, the mixing state of surfactant containing particles remains unclear due to the lack of direct measurements. Here, in-situ characterizations of mixing state for 20 kinds of submicron particles containing inorganic salts (NaCl and (NH<sub>4</sub>)<sub>2</sub>SO<sub>4</sub>) and atmospheric organic surfactants (organosulfates, organosulfonates, and dicarboxylic acids) were conducted upon relative humidity (RH) cycling by Environmental Scanning Electron Microscopy (ESEM). As RH increased, surfactant shells inhibited water diffusion exposing to inorganic core, leading to notably increased inorganic deliquescence RH (88.3–99.5%) compared with pure inorganic aerosol. Meanwhile, we directly observed obvious Ostwald ripening process, that is, the growth of larger crystals at the expense of smaller ones, in 6 among 10 NaCl-organic surfactants systems. As a result of water inhibition by organic surfactant shell, Ostwald ripening in all systems occurred at RH above 90%, which were higher than reported RH range for pure NaCl measured at 27°C (75–77%). As RH decreased, 8 systems underwent liquid-liquid phase separation (LLPS) before efflorescence, showing a strong dependence on organic molecular oxygen-to-carbon ratio (O:C). Quantitatively, LLPS was always observed when O:C ≤ 0.43 and was never observed when O:C > ~0.57. Separation RH (SRH) of inorganic salt-organic surfactant mixtures generally followed the trend of (NH<sub>4</sub>)<sub>2</sub>SO<sub>4</sub> < NaCl, which is consistent with their salting out efficiencies reported in previous studies. Solid Phase-phase separations were observed after efflorescence for systems without LLPS. Our results provide a unique insight into the consecutive mixing processes of the inorganic salt-organic surfactant particles, which would help improve our fundamental knowledge of model development on radiative effect.

30 Atmospheric particles are complex mixtures of multiple inorganic and organic matters (Pöschl, 2005). When relative  
31 humidity (RH) varies, particles can undergo phase transitions such as deliquescence (Peng et al., 2001), efflorescence  
32 (Takahama et al., 2007), and liquid–liquid phase separation (LLPS) (Martin, 2000), hence altering mixing state. The transition  
33 of aerosol mixing state can influence gas uptake, hygroscopicity, cloud condensation nuclei (CCN) activity, and radiative  
34 absorption (Riemer et al., 2019).

35 Upon hydration, previous studies suggested that different mixing state between inorganic and organic matters influence  
36 aerosol hygroscopic behaviours (e.g., deliquescence) and solar radiation (Peng et al., 2016; Li et al., 2021). For instance, Peng  
37 et al. (2016) observed ~~deliquescence RH of~~ internal mixed NaCl–oxalic acid ~~deliquesced~~ at 73% RH, being slightly lower than  
38 that of pure NaCl (75%) because of the interactions between inorganic and organic matters. However, Li et al. (2021) found a  
39 different deliquescence process if ammonium sulfate (AS) was coated by secondary organic aerosol, the organic shell firstly  
40 dissolved at ~50% RH but water uptake of the AS core was inhibited, leading to a higher deliquescence RH of AS (~83–90%).  
41 By cryogenic transmission electron microscopy (cryo–TEM), Zhang et al. (2022) directly observed collected particles from a  
42 rural site remained LLPS (inner inorganic p<sub>0</sub>hase and outer organic phase) between organic matter and inorganic salts when  
43 RH raised to  $75 \pm 2\%$  and  $86 \pm 2\%$ , but LLPS disappeared when RH increased to  $95 \pm 2\%$ . They later suggested that LLPS  
44 with higher ratio of organic coating thickness to black carbon size can drive black carbon from inorganic core to organic  
45 particle coatings, which could result in 18% radiative absorption overestimation of black carbon aerosols in climate models by  
46 assuming a core-shell particle structure.

47 Upon dehydration, phase separation has been frequently observed in ambient particles (You et al., 2012; Ting et al., 2018;  
48 Zhang et al., 2020; Zhang et al., 2022). For example, LLPS occurred at  $> 90\%$  RH for particles containing water extraction of  
49 collected atmospheric particles in Atlanta and simulations indicated that LLPS can decrease particle uptake of  $\text{N}_2\text{O}_5$  thus  
50 increase concentrations of gas–phase  $\text{NO}_3$  and  $\text{N}_2\text{O}_5$  (You et al., 2012). Factors contributing to LLPS, e.g. oxidation levels  
51 (Bertram et al., 2011; Song et al., 2017; Song et al., 2019), organic fraction (Ciobanu et al., 2009; Song et al., 2012a), inorganic  
52 species (You et al., 2013), and temperature (You and Bertram, 2015; Roy et al., 2020) have been discussed for some specific  
53 inorganic–organic or organic–organic systems in literature. Song et al. (2012b) and You et al. (2013) found LLPS always  
54 occurred for  $\text{O}:\text{C} < \sim 0.5$ , never occurred for  $\text{O}:\text{C} > 0.8$ , and when  $\text{O}:\text{C}$  was between 0.5 and 0.8, LLPS was depended on  
55 inorganic species. Organic fraction showed controversial effects on LLPS (Bertram et al., 2011; Song et al., 2012a) since  
56 Bertram et al. (2011) found a weak effect of organic fraction on LLPS for 8 out of 11 AS–organic systems but the rest systems  
57 exhibited a quantifiable dependence of separation RH (SRH) on organic fraction. You et al. (2013) reported SRH among out  
58 of 20 organics generally followed the trend of  $(\text{NH}_4)_2\text{SO}_4 \geq \text{NH}_4\text{HSO}_4 \geq \text{NaCl} \geq \text{NH}_4\text{NO}_3$ , which is consistent with  
59 ~~inorganic their previous reported~~ salting out efficiencies. Temperature did not strongly affect SRH between 253–290 K for  
60 AS–organics (O'brien et al., 2015; You and Bertram, 2015) and NaCl–organics systems (Roy et al., 2020). Recently, dry rate

61 (Altaf and Freedman, 2017; Altaf et al., 2018) and size effect (Freedman, 2020; Ott and Freedman, 2021; Ohno et al., 2023)  
62 on LLPS were found for submicron particles. Undergoing drying by slow-fast rate (~ 27% per minute), phase separation of  
63 AS-pimelic acid system occurred in larger particles (75 ~ 322 nm diameter), but smaller particles (below 25~135 nm diameter)  
64 were homogeneous. In slow drying rates (0.04 to 0.08% RH per second), particles with diameter below 43 nm were  
65 homogeneous but larger particles (28 ~ 629 nm) were mainly phase-separated (Altaf and Freedman, 2017). Freedman (2020)  
66 further explained that LLPS is scarcely occurred in smaller particles as smaller particles cannot overcome the energy barrier  
67 needed to form a new phase.

68 Dicarboxylic acids (Ruehl and Wilson, 2014), organosulfates (Bruggemann et al., 2020; Reed et al., 2022), and  
69 organosulfonates (Bruggemann et al., 2020; Guo et al., 2020) are important organic constituents in secondary organic aerosol.  
70 Primary emission and secondary transition were major sources of dicarboxylic acids and their mass contribution of  
71 dicarboxylic acids to total particulate carbon exceeds 10% (Römpf et al., 2006; Ho et al., 2010; Hyder et al., 2012).  
72 Organosulfates and organosulfonates, as significant reservoirs of sulfur, comprise an estimated 5%–30% of the total organic  
73 aerosol mass (Tolocka and Turpin, 2012; Reed et al., 2022). Above mentioned organics contain both hydrophilic (e.g., sulfo  
74 group) and hydrophobic groups (e.g., alkyl group), showing surface activity and causing bulk–surface partitioning (Noziere,  
75 2016; Ruehl et al., 2016), hence affecting individual aerosol morphology (Kwamena et al., 2010). However, mixing state of  
76 submicron inorganic salt-organic surfactant particles remain unclear due to the lack of direct measurements. Here, we directly  
77 observed mixing states of submicron particles containing inorganic salt and organic surfactant with varying organic volume  
78 fraction (OVF) upon humidity cycling by Environmental Scanning Electron Microscopy (ESEM). Our results could provide  
79 unique insights into the dynamic evolution of inorganic salt-organic surfactant~~inorganic=surfactant~~ particles under fluctuating  
80 atmospheric conditions.

## 81 **2 Materials and Methods**

### 82 **2.1 Chemicals–**

83 NaCl and AS were purchased from Sinopharm chemical reagent (purity ≥ 99.8%) and Sigma Aldrich (purity ≥ 99 %),  
84 respectively. The studied organic substances include 10 surface active organics (five organosulfonates, three organiosulfates  
85 and two dicarboxylic acids). The five organic sulfonates were sodium propane sulfonate (C<sub>3</sub>H<sub>7</sub>SO<sub>3</sub>Na), sodium butane  
86 sulfonate (C<sub>4</sub>H<sub>9</sub>SO<sub>3</sub>Na), sodium pentane sulfonate (C<sub>5</sub>H<sub>11</sub>SO<sub>3</sub>Na), sodium heptane sulfonate (C<sub>7</sub>H<sub>15</sub>SO<sub>3</sub>Na), sodium octane  
87 sulfonate (C<sub>8</sub>H<sub>17</sub>SO<sub>3</sub>Na). The three organic sulfates were sodium methyl sulfate (CH<sub>3</sub>SO<sub>4</sub>Na), sodium ethyl sulfate  
88 (C<sub>2</sub>H<sub>5</sub>SO<sub>4</sub>Na) and sodium octyl sulfate (C<sub>8</sub>H<sub>17</sub>SO<sub>4</sub>Na). Two dicarboxylic acids were pimelic acid (PA) and phenylmalonic acid  
89 (PhMA). Relevant properties of used chemicals were summarized in **Table 1**. These organic surfactants were of various  
90 solubilities, from sparingly soluble (e.g., 0.07 mol L<sup>-1</sup> for C<sub>8</sub>H<sub>17</sub>SO<sub>4</sub>Na) to highly soluble (e.g., 2.7-6 mol L<sup>-1</sup> for CH<sub>3</sub>SO<sub>4</sub>Na  
91 C<sub>4</sub>H<sub>9</sub>SO<sub>3</sub>Na). O:C ratios were from 0.38 to 4, covering most of the molar ratios in the atmosphere (0.1–1.0) (You et al., 2013).

92 The studied organic substances contain functional groups such as sulfonates, sulfates, carboxylic acids and aromatics, which  
 93 were universally detected in atmospheric aerosol samples (Takahama et al., 2007).

94

95 **Table 1** Organic surfactants and their relevant properties investigated in this study.

Species	Compounds	Formula	*Solubility (mol L <sup>-1</sup> )	O:C	Purity	Supplier
Organic sulfonate	Sodium propane sulfonate	C <sub>3</sub> H <sub>7</sub> SO <sub>3</sub> Na	<u>2.5</u>	1.00	>98%	Aladdin
	Sodium butane sulfonate	C <sub>4</sub> H <sub>9</sub> SO <sub>3</sub> Na	<u>2.4</u>	0.75	≥99%	Aladdin
	Sodium pentane sulfonate	C <sub>5</sub> H <sub>11</sub> SO <sub>3</sub> Na	0.8	0.60	98%	Aladdin
	Sodium heptane sulfonate	C <sub>7</sub> H <sub>15</sub> SO <sub>3</sub> Na	<u>0.6</u>	0.43	98%	Macklin
	Sodium octane sulfonate	C <sub>8</sub> H <sub>17</sub> SO <sub>3</sub> Na	<u>0.07</u>	0.38	≥99%	Macklin
Organic sulfate	Sodium methyl sulfate	CH <sub>3</sub> SO <sub>4</sub> Na	2.6	4.00	98%	Energy Chemical
	Sodium ethyl sulfate	C <sub>2</sub> H <sub>5</sub> SO <sub>4</sub> Na	<u>1.5</u>	2.00	98%	Meryer
	Sodium octyl sulfate	C <sub>8</sub> H <sub>17</sub> SO <sub>4</sub> Na	<u>0.2</u>	0.50	99%	Rhawn
Dicarboxylic acid	Pimelic acid (PA)	C <sub>7</sub> H <sub>12</sub> O <sub>4</sub>	0.3	0.57	99%	Macklin
	Phenylmalonic acid (PhMA)	C <sub>9</sub> H <sub>8</sub> O <sub>4</sub>	<u>0.2</u>	0.44	98%	Aladdin

96

97 \* <https://comptox.epa.gov/> (last access: 12-19 March, 2023)

## 98 2.2 Aerosol generation and collection

99 The process of aerosol generation and collection was detailedly described by Xiong et al. (2022). In brief, particles were  
 100 nebulized from solutions of organic and inorganic matters (~5 g L<sup>-1</sup>) mixed with deionized water (Millipore, resistivity = 18.2  
 101 MΩ). After drying (RH < 15%) by a silica-gel diffusion dryer, particles were deposited with an eight stage non-viable particle  
 102 sizing sampler (Models BGI20800 Series, BGI Incorporation) onto 400 mesh copper grids coated with carbon films  
 103 (Zhongjingkeyi Films Technology Co. Ltd.). Copper grids were mounted on the 7<sup>th</sup> stage, selecting particles with aerodynamic  
 104 size of 0.7–1 μm. Collected samples were stored under dry condition (RH < 10%) and were immediately characterized within

105 24 hours to avoid possible sample aging.

### 106 2.3 Mixing state observation

107 Optical microscopy (Ciobanu et al., 2009; Bertram et al., 2011; Song et al., 2012a, b; You et al., 2013), microfluidic device  
108 (Roy et al., 2020), Cryo-TEM (Veghte et al., 2014; Freedman, 2020; Ott and Freedman, 2021; Ott et al., 2021; Zhang et al.,  
109 2022), ESEM (O'Brien et al., 2015), optical tweezer (Stewart et al., 2015; Tong et al., 2022) and F-AFT (Fluorescence aerosol  
110 flow tube) (Ohno et al., 2021; Ohno et al., 2023) were reported methods for detecting aerosol mixing state in the literature.  
111 Optical microscopy and microfluidic device were commonly used direct method for substrate-supported droplets but was  
112 limited by size range (at least dozens of micrometers). Optical tweezer and F-AFT could investigated LLPS in a levitated  
113 micrometer and sub-micrometer droplet, respectively, but are indirect ways, although no distinct differences when comparing  
114 to substrate-supported droplets (Ohno et al., 2023). Cryo-TEM and ESEM could detect mixing state in sub-micrometer scale  
115 but damage caused by electron beam may exist (depend on chemistry and beam parameters settings). Ott et al. (2021) give  
116 some useful suggestions in minimize the damage, e.g., decreasing exposure dose and time to particles.

117 ~~M~~Mixing state was observed by Environmental Scanning Electron Microscopy (ESEM, Thermo Quattro S) with a  
118 temperature-controlled stage. The RH in chamber was varied between 0.1 to ~ 25 °C, and controlled by adjusting the  
119 temperature ( $\pm 0.1$  °C) at a predefined pressure (610 Pa). ~~Temperature varied between 0.1 to ~ 25 °C, which has negligible~~  
120 ~~influence on the LLPS of AS-organic (O'Brien et al., 2015; You and Bertram, 2015) and NaCl-organic systems (Roy et al.,~~  
121 ~~2020).~~ In each experiment, particles with lateral dimensions of ~ 1  $\mu\text{m}$  were selected first (based on the deposition, volume-  
122 equivalent size was smaller than 1  $\mu\text{m}$ ). Then the RH raised from low (~ 30%) to high condition (~100%) at the change rate  
123 of 2–3% RH min<sup>-1</sup>. High RH lasted for at least 5 minutes for equilibrium, promising complete dissolution (O'Brien et al., 2015).  
124 With increased RH, most selected particles grew larger to several micrometers before subsequent LLPS experiment. Then, RH  
125 decreased to dry condition at similar change rate. Negligible influence on the LLPS of AS-organic (O'Brien et al., 2015; You  
126 and Bertram, 2015) and NaCl-organic systems (Roy et al., 2020) in micrometre scale (from several micrometers to dozens of  
127 micrometers). Then, RH decreased to dry condition at similar change rate. ~~Temperature varied between 0.1 to ~ 25 °C, which~~  
128 ~~has negligible influence on the LLPS of AS-organic and NaCl-organic systems.~~ Cloud parcel modelling suggests that  
129 atmospheric RH fluctuations typically occur from 0 to 3.6% min<sup>-1</sup> (Pöhlker et al., 2014). Therefore, we assume that the water  
130 uptake in our experiments approximates atmospheric conditions (Shiraiwa et al., 2013). Images of mixing states during the  
131 whole RH period were acquired at an electron acceleration voltage of 30 kV. The detector used for the ESEM imaging was a  
132 scanning transmission electron detector. The images were recorded with line scanning rates of 3–5  $\mu\text{s}$  to minimize the possible  
133 beam damage (Supporting information, O'Brien et al., 2015). The varying range of RH value between two consecutive pictures  
134 were mostly 0.2–0.4% RH (very narrow), in order to capture the possible quick transitions of mixing states. Each image in our  
135 study contained at least 5 particles (or droplets) to ensure the ESEM reproducibility and decrease the uncertainty. In addition,  
136 we have repeated some of the experiment (e.g., in the RH decreasing period) for reproducibility validation, and the results

137 showed good consistence (Fig. S1). Each image contained at least 5 particles.

## 138 3 Results and Discussion

### 139 3.1 Mixing states upon hydration

140 Deliquescence RH (DRH) and Efflorescence RH (ERH) of pure NaCl (Fig. 1a–d and Fig. S1a–S2a–b) and AS particles  
141 (Fig. 2a–d and Fig. S1e–S2c–d) were firstly tested via the experimental setup. DRH of NaCl and AS were observed at  $80.9 \pm$   
142  $0.1\%$  (literature:  $77 \pm 1\%$  (Pöhlker et al., 2014)) and  $82.1 \pm 0.6\%$  (literature:  $82.0\%$  (Onasch et al., 1999)). ERH of NaCl and  
143 AS were  $48.3 \pm 0.4\%$  (literature:  $48 \pm 2\%$  (Zeng et al., 2014)) and  $30.7 \pm 0.9\%$  (literature:  $31 \pm 1\%$  (Cheng and Kuwata, 2023)).  
144 Generally, the experimental DRH and ERH values correspond well with those in literature, confirming the reliability of the  
145 experimental setup. DRH of NaCl showed slight deviation by about nearly 4%, which could be explained by kinetic effects  
146 when the system had not reached full equilibrium (Pöhlker et al., 2014). Before deliquescence, the substrate-supported NaCl  
147 and AS particles both showed substantial water uptake, forming an aqueous halo around a solid core. Similar observational  
148 results of NaCl and AS have been reported, and could be explained by interactions at the sample/substrate interface, which  
149 plays an important role in such gradual phase transition as additional energy term (Wise et al., 2008; Pöhlker et al., 2014).

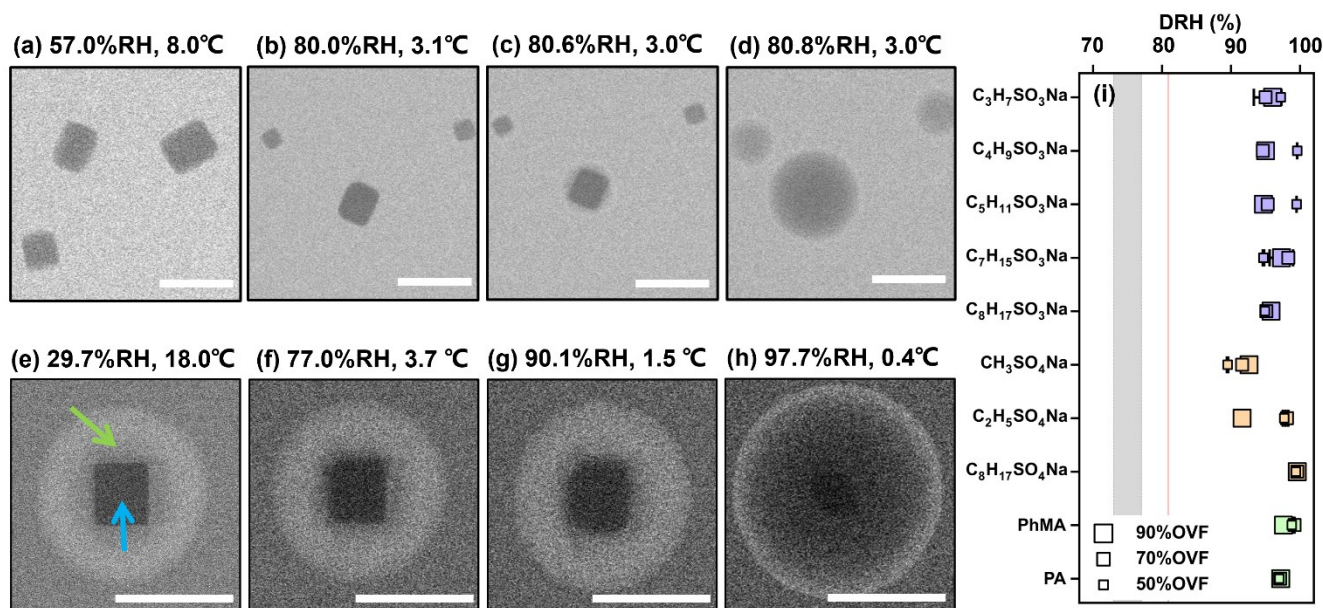
150 **Figure 1e and Fig. 2e** illustrate the two separated phases with dark core (blue arrow) and bright shell (green arrow) of  
151 dry deposited NaCl–C<sub>2</sub>H<sub>5</sub>SO<sub>4</sub>Na and AS–C<sub>2</sub>H<sub>5</sub>SO<sub>4</sub>Na particles. The dark cores are indicated to be inorganics, because darker  
152 regions are characteristic of areas with higher atomic number elements (e.g., Cl) and/or a thicker sample region (Laskin et al.,  
153 2006; O'brien et al., 2015). Phase separations with core–shell structure were observed for all studied inorganic salt–organic  
154 surfactant~~inorganic–surfactant~~ systems. This may be attributed to the size range of particles we investigated (0.7–~1 μm with  
155 dry lateral dimension), since inorganic salt–organic surfactant~~inorganic–surfactants~~ particles with such size range might  
156 overcome the energy barrier needed to form a new phase (Altaf and Freedman, 2017; Altaf et al., 2018; Freedman, 2020; Ott  
157 and Freedman, 2021). According to results in Freedman (2020), morphology of most systems were found size-dependent,  
158 where large particles were phase-separated and small particles were homogeneous. Furthermore, all systems (e.g. AS–PA and  
159 AS–succinic acid systems) with dry diameters larger than 0.7 μm were observed phase-separated no matter the occurrence of  
160 size dependence (Altaf and Freedman, 2017). Freedman (2020) expected that phase-separation could be attributed by  
161 nucleation and growth, therefore larger particles tended to be phase-separated morphology. In another study, Ohno et al. (2021)  
162 also found that LLPS occurred at lower RH in smaller droplet (70 – 190 nm) than in larger droplet (260 – 370 nm).

163 When RH increased from dry, as organic phase slowly absorbed water, NaCl and AS cores were not fully dissolved at  
164 RH of 90.1% and 91.7% (Fig. 1g and Fig. 2g), respectively, being notably higher than their DRH. The phenomenon was found  
165 for all NaCl–organic surfactant and AS–organic surfactant systems and the DRH of the inorganic salts were ranged in  
166 88.3–99.5% (Fig. 1i and Fig. 2i). Laskina et al. (2015) measured the DRH of pure AS and NaCl at submicrometer (100 nm)  
167 and supermicrometer (3–10 μm) size ranges by hygroscopic tandem differential mobility analyzers (HTDMA) and

168 MicroRaman Spectroscopy, respectively, and the deviations between them were both within 3%, indicating that DRH of pure  
169 AS and NaCl showed weak size dependence (> 100 nm). In addition, Cheng and Kuwata (2023) used low-temperature  
170 hygroscopicity tandem differential mobility analyzer (Low-T HTDMA) and observed consistent DRH of NaCl and AS within  
171 experimental error under temperature ranged in -10 °C to 22.5 °C, suggesting that the DRH of NaCl and AS experience a  
172 neglect temperature dependence. According to the above-mentioned studies, DRH of pure AS and NaCl displayed weak  
173 dependence on size (> 100 nm) and temperature, and we therefore concluded that surfactant shell inhibits water diffusion  
174 exposing to inorganic cores, resulting in delays of deliquescence of inorganic cores. ~~According to the above-mentioned studies,~~  
175 ~~DRH of pure AS and NaCl showed weak size dependence (> 100 nm) and temperature dependence in our experiment, and we~~  
176 ~~therefore concluded that surfactant shell inhibits water diffusion exposing to inorganic cores, resulting in delays of~~  
177 ~~deliquescence of inorganic cores.~~ The inhibition of surfactant shell could be triggered by increased viscosity with raised RH,  
178 since reported studies have reported that organic shells can transform from solid to semisolid with high viscosity at wet  
179 condition (Zhang et al., 2018). In a RH-constrained lab study at constant room temperature, Li et al. (2021) also observed  
180 organic coating of secondary organic aerosol (oxidizing  $\alpha$ -pinene) started to deliquesce first, but the phase changes of AS cores  
181 from solid to liquid took place at 83–90% RH, lower than those in the current study. This was possibly caused by the water  
182 diffusion coefficient through organic phase, which could be affected by organic species and environment parameters such as  
183 temperature. Given by Nguyen et al. (2017), the diffusion coefficient of a water molecule through an organic shell could be  
184 decreased by lower temperature. In the current study, higher RH in the ESEM chamber was achieved by decreasing temperature,  
185 thus might decrease diffusion coefficient of water in organic surfactant and lead to higher DRH than those in Li et al. (2021).  
186 Previous study and the current work indicated the phenomenon (water inhabitation by organic coating) to be a common and  
187 important procedure in affecting ambient aerosol hygroscopicity, because inorganic–organic core–shell structures were  
188 ubiquitous observed in field (Li et al., 2016; Unga et al., 2018; Xu et al., 2020; Li et al., 2021; Wang et al., 2021; Zhang et al.,  
189 2022). Though the water inhabitation of organic shell in the current study was observed at temperature much lower than room  
190 temperature, it is meaningful and may affect aerosol properties in some special area such as polar regions (Lambert et al., 2013;  
191 Kirpes et al., 2022; Zavaacka et al., 2022) or winter time period (Xu et al., 2021; Zhang et al., 2021) where are characteristic  
192 with low-temperature environment.

193 As previous study believed that deliquescence on hydration for inorganics independent of circumstances, **Fig. 3** illustrates  
194 an unexpected phase transition of NaCl cores coated with  $C_2H_5SO_4Na$  (70% OVF). As shown in **Fig. 3a**, a droplet with several  
195 NaCl cores was observed at 97.0% RH since discussed above that organic shell inhibits water diffusion. NaCl cores in droplet  
196 were a bigger one (marked by white square) and the rest were smaller. When RH gradually raised (**Fig. 3b–c**), as smaller NaCl  
197 cores serially deliquesced and dissolved, the size of the bigger NaCl core surprisingly increased, indicating a simultaneous  
198 NaCl recrystallization at the expense of smaller ones (i.e., Ostwald ripening) (Boistelle and Astier, 1988). After other small  
199 particles totally dissolve, the bigger NaCl core deliquesced and fully dissolved at 99.5% RH (**Fig. 3d**). A previous study  
200 reported “efflorescence upon hydration” for 1:1 mixed NaCl-gluconic acid and AS-gluconic acid by optical tweezer (Zhu et

201 al., 2022). Based on IR spectrum, they found the coexistence of partial efflorescence mixed state, ultraviscous state and liquid  
 202 state during “efflorescence upon hydration” period, indicating an unstable crystal and concentrated liquid state of NaCl. In this  
 203 circumstance, Ostwald ripening can take place. Ostwald ripening was triggered by the decrease of total system free energy,  
 204 since dissolved small and effloresced big crystals reduce the total system free energy (Voorhees, 1985). We directly and  
 205 observed obvious Ostwald ripening processes in 6 among 10 NaCl–organic surfactants systems. As a results of water inhibition  
 206 by surfactant shell discussed above, Ostwald ripening here all occurred at RH above 90%, which were notably higher than  
 207 reported 75%–77% for pure NaCl measured by X-ray microspectroscopy at 27°C (Pöhlker et al., 2014).  
 208



209 **Figure 1.** ESEM images of (a–d) pure NaCl and (e–h) NaCl–C<sub>2</sub>H<sub>5</sub>SO<sub>4</sub>Na (70% OVF) with different RH. Blue and green  
 210 arrows indicate the inorganic phase and organic phase, respectively. The RH value that NaCl core fully dissolved (DRH) for  
 211 NaCl–organic surfactant systems with different OVF (i). Grey area in (i) covers DRH range of NaCl in the literature obtained  
 212 from Peng et al. (2022). Red line indicates the measured average DRH of pure NaCl (80.9 ± 0.1%). Scale bars in (a–h) were 1  
 213 μm. ESEM images of (a–d) pure NaCl and (e–h) NaCl–C<sub>2</sub>H<sub>5</sub>SO<sub>4</sub>Na (70% OVF) with different RH. Blue and green arrows  
 214 indicate the inorganic phase and organic phase, respectively. DRH values of inorganic core for NaCl–surfactant systems (i).  
 215 Grey area represents DRH range of NaCl obtained from Peng et al. (2022). Red line indicates the measured DRH of pure NaCl  
 216 (80.9 ± 0.1%). Scale bars were 1 μm.  
 217  
 218



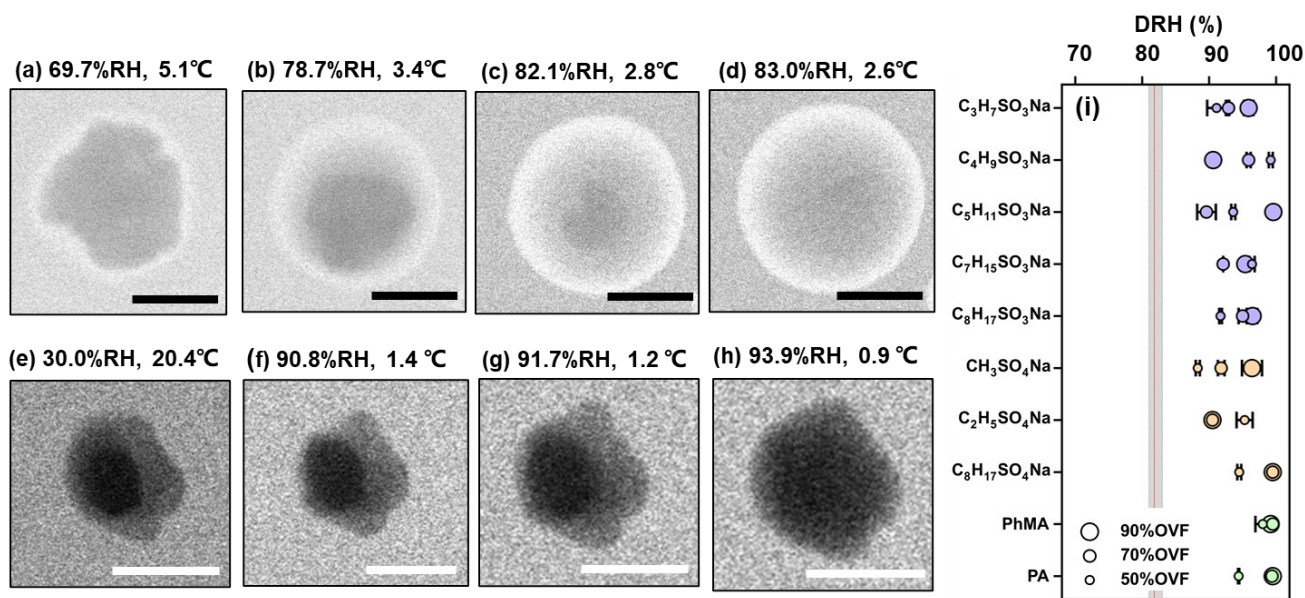
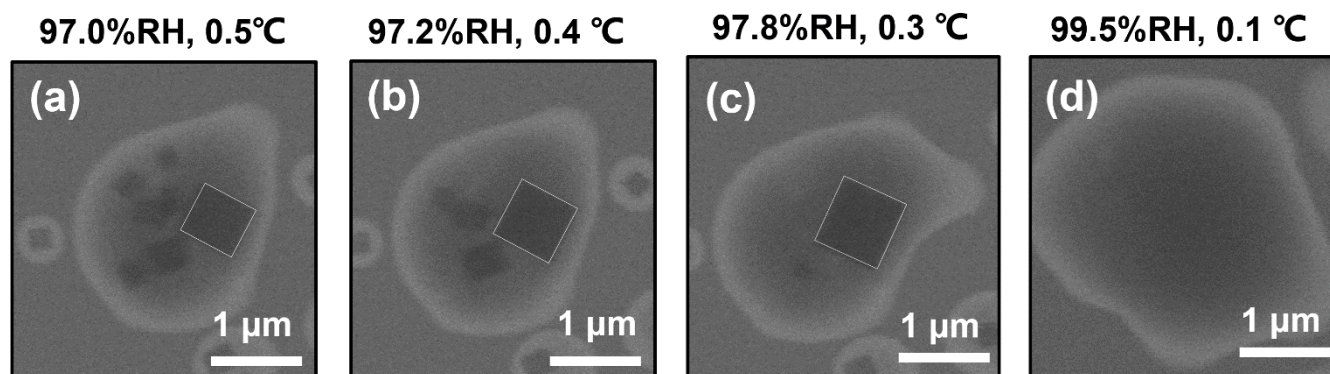


**Figure 2.** ESEM images of (a–d) pure AS and (e–h) AS–C<sub>2</sub>H<sub>5</sub>SO<sub>4</sub>Na (50% OVF) with different RH. Blue and green arrows indicate the inorganic phase and organic phase, respectively. The RH value that AS core fully dissolved (DRH) for AS–organic surfactant systems with different OVF (i). Grey area in (i) covers DRH range of AS in the literature obtained from Peng et al. (2022). Red line indicates the measured average DRH of pure AS (82.1 ± 0.6%). Scale bars in (a–h) were 1 μm. ESEM images of (a–d) pure AS and (e–h) AS–C<sub>2</sub>H<sub>5</sub>SO<sub>4</sub>Na (50% OVF) with different RH. Blue and green arrows indicate the inorganic phase and organic phase, respectively. (i) DRH values of inorganic core for AS–surfactant systems. Grey area represents DRH range of AS obtained from Peng et al. (2022). Red line indicates the measured DRH of pure AS (82.1 ± 0.6%). Scale bars in (a–h) were 1 μm.



232

233 **Figure 3.** ESEM images of Ostwald ripening for NaCl-C<sub>8</sub>H<sub>17</sub>SO<sub>4</sub>Na (50% OVF) particle. White square indicates the biggest  
234 NaCl core (assumed square) in droplet. The biggest NaCl grew larger (recrystallization) while the small NaCl cores dissolved.

235

## 236 3.2 Mixing states upon dehydration

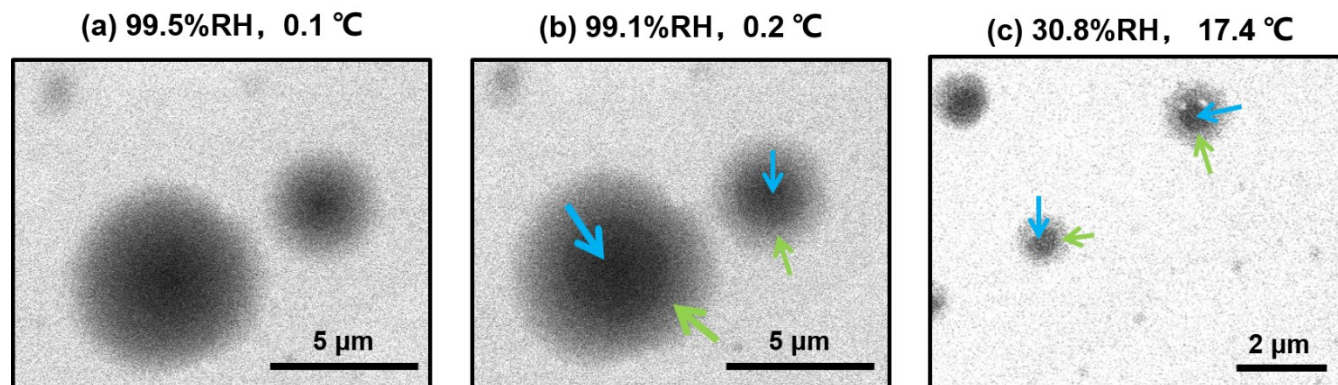
### 237 LLPS

238 In Fig. 4a, AS-C<sub>8</sub>H<sub>17</sub>SO<sub>4</sub>Na (~~50% OVF~~) was homogeneous under RH of 99.5%. When RH decreased to 98.2%, the  
239 particles showed two separated liquid phases (i.e., LLPS) with a dark inner phase and a light outer phase (Fig. 4b), which were  
240 highlighted by the blue and green arrows. In addition, the AS-C<sub>8</sub>H<sub>17</sub>SO<sub>4</sub>Na remained LLPS when RH continue to decline until  
241 efflorescence of inner inorganic phase occurred (Fig. 4c). In our study, 8 among 20 chemical systems underwent LLPS,  
242 including 4 AS-organic surfactant systems and 4 NaCl-organic surfactant systems. ~~Fig. 5 illustrates the relationship  
243 between LLPS occurrence and molar ratios (O:C and H:C) of the surface-active organics, as well as reported results  
244 of other binary inorganic-organic systems in You et al. (2013) and O'brien et al. (2015). Firstly, no trend was observed  
245 between LLPS occurrence and H:C of the organics. This was consistent with results in previous studies (Bertram et al.,  
246 2011; Song et al., 2012a; You et al., 2013). An apparent trend was found between O:C ratio and LLPS occurrence for  
247 different systems, that is, LLPS of inorganic-organic particles were more likely to occurred when O:C ratio was low.  
248 Quantitatively, LLPS was always observed for O:C < 0.4 and never observed for O:C ≥ 0.57 (grey area) was found for  
249 NaCl-surfactants and AS-surfactants systems. You et al. (2013) reported that LLPS always occurred for O:C < 0.5 and  
250 was never observed for O:C ≥ 0.8 for NaCl-organics and AS-organics with organic to inorganic mass ratio of 2 ± 0.1,  
251 which was different from our results. This could be attributed to the different chemical systems. Fig. 5 illustrates the  
252 relationship between LLPS occurrence and molar ratios (O:C and H:C) of the surface-active organics, as well as reported  
253 results of other binary inorganic salt-organic systems in literature (Bertram et al., 2011; You et al., 2013; You and Bertram,  
254 2015). In our study, LLPS always occurs when the O:C ratio is below 0.43 (yellow dashed line in Fig. 5) for NaCl-organic  
255 surfactant and AS-organic surfactant droplets. This value was close to the reported values in You et al. (2013) (~0.5). However,  
256 in their results, LLPS was never observed when O:C was above ~0.8 (grey dashed line in Fig. 5) (Bertram et al., 2011; Song  
257 et al., 2012b; You et al., 2013), which was higher than that in our experiment (0.57). We ascribe this to the insufficient chemical  
258 systems in our experiment (10 systems), which was notably smaller than in previous studies (over 30). As a result, the bounds  
259 of O:C determining LLPS were not changed if our results were added in previous studies such as You et al. (2013) and Song  
260 et al. (2012b).~~

261 In order to analyze the effect of inorganic salts in LLPS, we compared SRH of systems which contained same organic  
262 matters but different inorganic salts. Results showed that SRH of AS-C<sub>8</sub>H<sub>17</sub>SO<sub>4</sub>Na (70% OVF), AS-C<sub>8</sub>H<sub>17</sub>SO<sub>3</sub>Na (90% OVF),  
263 AS-PhMA (90% OVF) and AS-PA (90% OVF) were 98.7 ± 0.5%, 81.3 ± 1.2%, 97.9 ± 1.0% and 98.5 ± 0.8%, and were all  
264 notably higher than SRH of corresponding NaCl-containing systems (92.5 ± 3.9%, 56.4 ± 1.2%, 85.6 ± 3.6% and 66.7 ± 0.8%),  
265 respectively. This was attributed to different salting out efficiency of inorganic salts, since You et al. (2013) found the SRH of  
266 inorganic-organic mixtures followed the trend of (NH<sub>4</sub>)<sub>2</sub>SO<sub>4</sub> ≥ NH<sub>4</sub>HSO<sub>4</sub> ≥ NaCl ≥ NH<sub>4</sub>NO<sub>3</sub>, which were generally consistent  
267 with their salting out efficiency.

268 The measured SRH values as a function of OVF are plotted in **Fig. 6**. AS-C<sub>8</sub>H<sub>17</sub>SO<sub>4</sub>Na showed SRH of  $98.7 \pm 0.5\%$   
269 when OVF was 70%, higher than those of 50% OVF ( $82.1 \pm 1.6\%$ ) and 90% OVF ( $80.0 \pm 0.9\%$ ). However, the phenomenon  
270 was totally different from that of AS-C<sub>8</sub>H<sub>17</sub>SO<sub>3</sub>Na, which showed lower SRH with 70% OVF ( $62.2 \pm 2.6\%$ ) than those of 50%  
271 OVF ( $69.6 \pm 1.0\%$ ) and 90% OVF ( $81.3 \pm 1.2\%$ ). Therefore, the above results indicated controversial effect of OVF on SRH  
272 (Bertram et al., 2011; Song et al., 2012a).

273

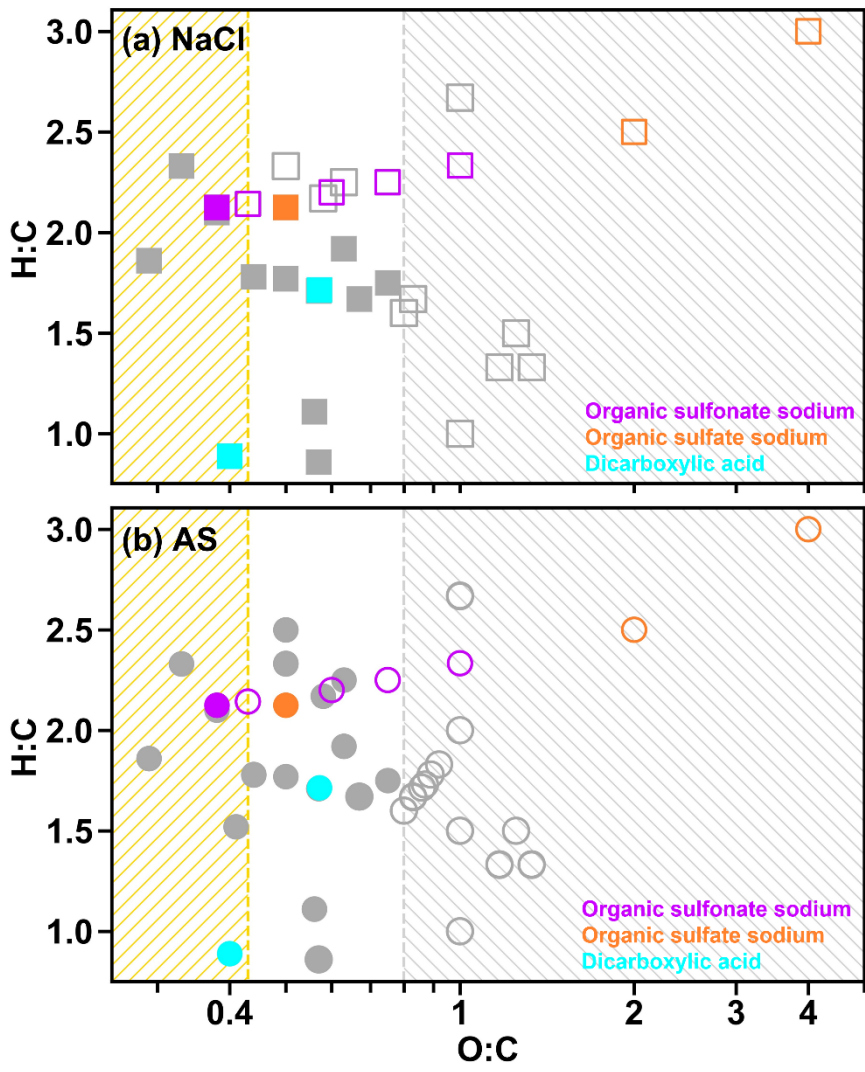


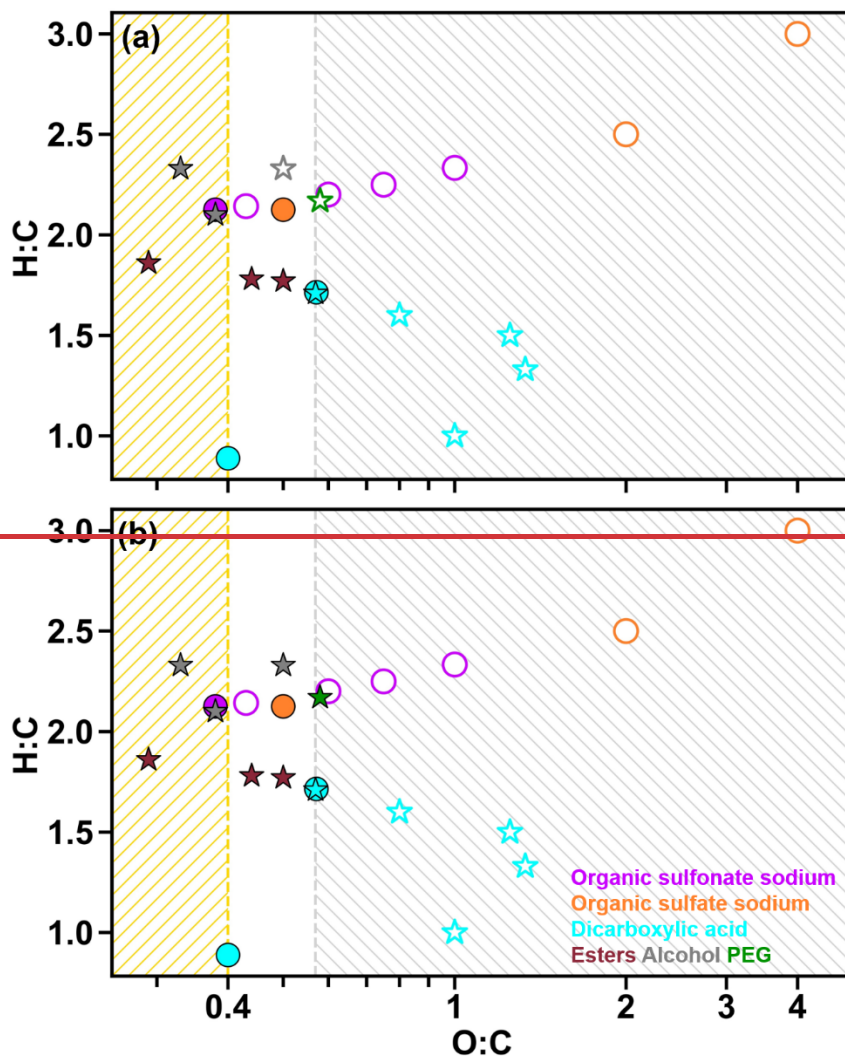
274

275

276 **Figure 4.** ESEM images of (a) homogeneous AS-C<sub>8</sub>H<sub>17</sub>SO<sub>4</sub>Na particles (~~50~~70% OVF) underwent (b) LLPS and (c)  
277 efflorescence.

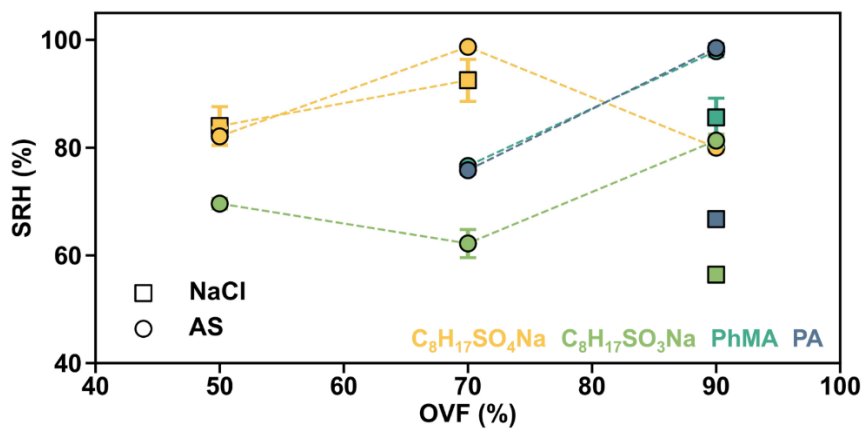
278





280  
 281 **Figure 5.** Van Krevelen Diagram for the mixed inorganic-surfactants particles in the current study (symbols in red, orange  
 282 and cyan): (a) NaCl-organic surfactant and (b) AS-organic surfactant systems. Solid symbols indicate that LLPS was observed  
 283 for particles with at least one OVF, while hollow symbols indicate that LLPS was not observed for particles with all OVFs.  
 284 Symbols in grey in (a) and (b) were results obtained from Bertram et al. (2011), You et al. (2013) and You and Bertram (2015).  
 285 Yellow-hatched region ( $O:C < 0.43$ ) means that LLPS observed in all investigated systems, while grey-hatched region ( $O:C >$   
 286  $0.8$ ) means no LLPS detected in any of the investigated systems. Van Krevelen Diagram for the mixed inorganic-organic  
 287 particles in the current study (marked as circles): (a) NaCl-containing systems and (b) AS-containing systems. Solid symbols  
 288 indicate that LLPS was observed for particles with at least one OVF, while hollow symbols indicate that LLPS was not  
 289 observed for particles with all tested OVFs. Stars indicate data obtained from You et al. (2013) and O'brien et al. (2015). PEG

290 represents polyethylene glycol.



291  
292 **Figure 6.** Summary of SRH results as a function of OVF for inorganic-surfactant particles.  
293

295 For mixed systems without undergoing LLPS, we found they were separated with distinct core-shell phases from  
296 homogeneous morphology at low RH. However, this phase transition was different from LLPS, since the inner phase was with  
297 irregular shape (LLPS occurred with rounded inner liquid phase), which was attributed to the efflorescence progress of  
298 inorganic salt (Fig. 7). Therefore, we termed it solid phase separation. The efflorescence RH (ERH) of inner inorganic salt,  
299 therefore, was the solid phase separation RH.

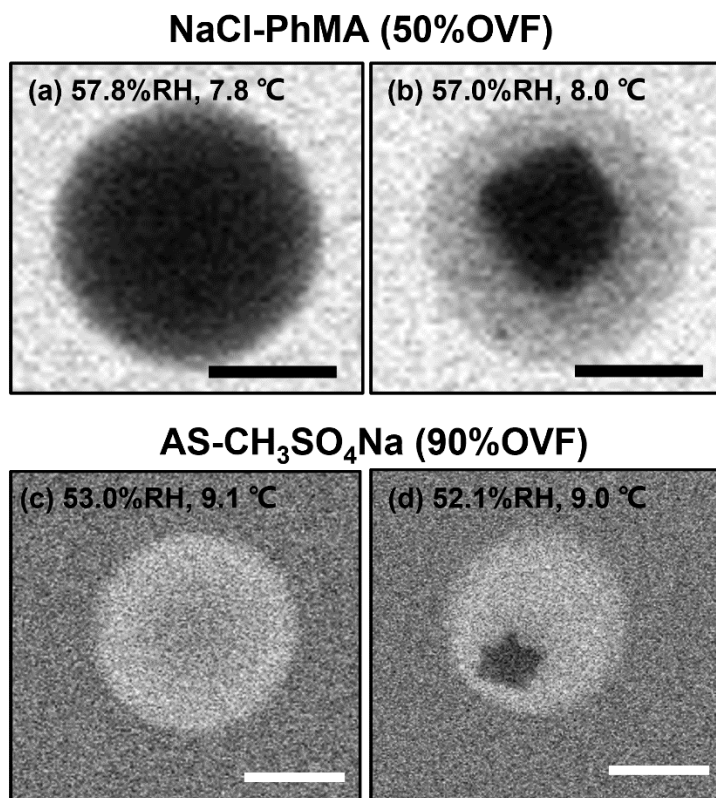
300 In Fig. 8a, ERH of NaCl-organic surfactant particles with 50%, 70% and 90% OVF were ranged in 47.0–61.8%, which  
301 was higher than the measured ERH ( $48.3 \pm 0.4\%$ ) and reported ERH range of pure NaCl (41–51%) (Peng et al., 2022). This  
302 could be explained by the interaction between organic and inorganic matters. For example, Ghorai et al. (2014) found an acid  
303 displacement reaction in NaCl-glutaric acid systems, which was driven by gaseous HCl liberation and causing chloride  
304 depletion. Such interactions of chloride depletion may facilitate efflorescence transitions, resulting in efflorescence at ~ 68%  
305 RH and ~ 60% RH, respectively, for internally mixed NaCl-glutaric acid particles with molar ratios of 1:3 and 1:1. Higher  
306 ERH could also be attributed to heterogeneous nucleation initiated by chemical purities (Choi and Chan, 2002). Choi and Chan  
307 (2002) observed 54.4% ERH for a 1:1 mixed NaCl-glutaric acid, and they explained that insoluble additives crystallized and  
308 formed nuclei for the heterogeneous efflorescence of inorganic salts, leading to their higher ERH values.

309 As for AS-organic surfactant systems (Fig. 8b), efflorescence was observed for 27 among 30 aerosol samples. We did  
310 not observe distinct occurrence of efflorescence for the rest 3 samples, and 2 samples among 3 were with 90% OVF, which  
311 could be explained by the possible loss of AS when it was persistently exposed to electronic beam (Posfai et al., 2013; O'brien  
312 et al., 2015), especially for particles in which inorganic fractions were small (i.e., high OVF). ERH values of AS-organic  
313 surfactant particles with 50%, 70%, and 90% OVF ranged in 31.2–46.6%, showing a close result to the reported ERH of pure  
314 AS (30–48%) (Peng et al., 2022), but higher than the measured ERH ( $30.7 \pm 0.9\%$ ). The potential cause may be the  
315 heterogeneous crystallization of AS on organic salts (Wang et al., 2019; Yang et al., 2019; Ma et al., 2021). For example, Wang  
316 et al. (2019) investigated the efflorescence of AS in AS-sodium oxalate and found SRH values were 48.9% and 55.3% with  
317 organic-inorganic mole ratios of 1:1 and 3:1, respectively, which were higher than that of pure AS (47.5%). Likely, Yang et al.  
318 (2019) also observed that the initial ERH of AS rose to 47.7% and 62% for inorganic mole ratios 1:3 and 1:1 AS-sodium  
319 pyruvate mixtures, respectively.

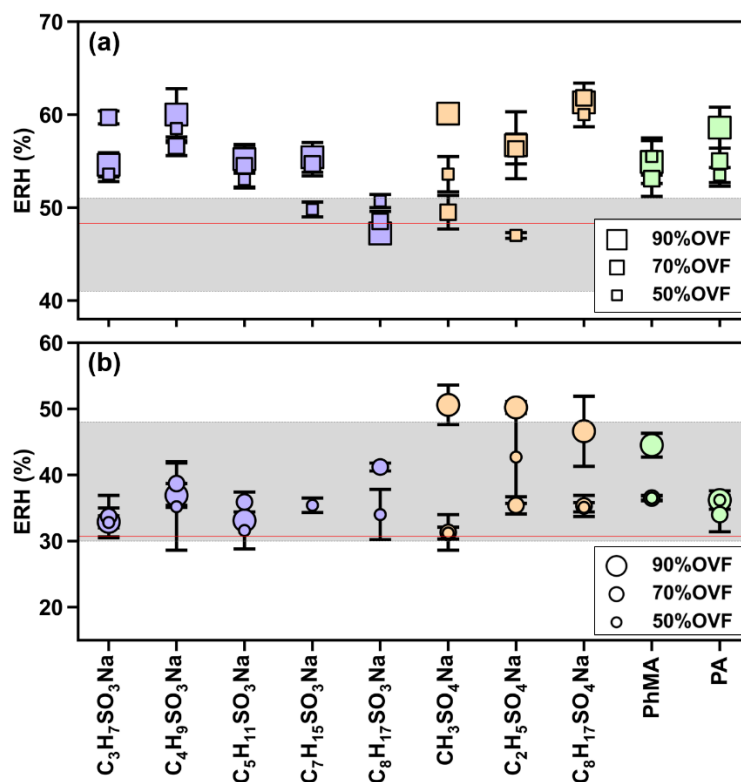
320 solid phase after obvious efflorescence of inorganic salts (e.g., AS-C<sub>2</sub>H<sub>5</sub>SO<sub>4</sub>Na and NaCl-C<sub>2</sub>H<sub>5</sub>SO<sub>4</sub>Na mixture shown  
321 in Fig. S2). In Fig. 7a, ERH of NaCl-surfactant particles with 50%, 70% and 90% OVF were ranged in 47.0–61.8%, which  
322 was higher than the measured ERH ( $48.3 \pm 0.4\%$ ) and reported ERH range of pure NaCl (41–51%) (Peng et al., 2022). As for  
323 AS-surfactant systems (Fig. 7b), efflorescence was observed for 27 among 30 aerosol samples. We did not observe distinct  
324 occurrence of efflorescence for the rest 3 samples, and 2 samples among 3 were with 90% OVF, which could be explained by  
325 the possible loss of AS when it was persistently exposed to electronic beam (Posfai et al., 2013; O'brien et al., 2015), especially  
326 for particles in which inorganic fractions were small (i.e., high OVF). ERH values of AS-surfactants particles with 50%, 70%,



327 and 90% OVF ranged in 31.2–46.6%, showing a close result to the reported ERH of pure AS (30–48%) (Peng et al., 2022),  
328 but higher than the measured ERH ( $30.7 \pm 0.9\%$ ). The higher efflorescence RH of inorganic-surfactant systems could be  
329 explained by the substrate-particle interactions. Ghorai et al. (2014) found an acid-displacement reaction in glutaric acid–NaCl  
330 systems, which was driven by gaseous HCl liberation and causing chloride depletion. Such interactions of chloride depletion  
331 may facilitate efflorescence transitions, resulting in efflorescence at ~68% RH and ~60% RH, respectively, for internally  
332 mixed NaCl–glutaric acid particles with molar ratios of 1:3 and 1:1. Higher ERH could also be attributed to heterogeneous  
333 nucleation initiated by chemical purities (Choi and Chan, 2002). Choi and Chan (2002) observed 54.4% ERH for a 1:1 mixed  
334 NaCl–glutaric acid, and they explained that insoluble additives crystallized and formed nuclei for the heterogeneous  
335 efflorescence of inorganic salts, leading to their higher ERH values.



336  
337  
338 **Figure 7.** ESEM images of solid phase separation for (a–b) NaCl–PhMA and (c–d) AS–CH<sub>3</sub>SO<sub>4</sub>Na systems. The scale bars  
339 in (a–d) were 500 nm.  
340



342

343 **Figure 78.** Measurements of efflorescence relative humidity (ERH) of (a) NaCl-organic surfactant and (b) AS-organic  
 344 surfactant particles. The grey areas in (a) and (b) indicate the efflorescence RH range of NaCl (41–51%) and AS (30–48%)  
 345 obtained from Peng et al. (2022). Red lines in (a) and (b) represent the measured average ERH of pure NaCl ( $48.3 \pm 0.4\%$ )  
 346 and AS ( $30.7 \pm 0.9\%$ ).

### 347 3.3 Atmospheric implication

348 Dicarboxylic acids, organosulfates, and organosulfonates are important surface-active organic constituents in secondary  
 349 organic aerosol. Few studies comprehensively studied their mixing state upon fluctuating RH cycling, which is a simulate of  
 350 real atmospheric condition. In this work, we concluded that mixing state affected interactions of inorganic salt with water.  
 351 Since common assumptions in chemical transport models (including ISORROPIA-II (Fountoukis and Nenes, 2007), EQSAM  
 352 (Metzger et al., 2002a; Metzger et al., 2002b), and MOSAIC (Zaveri et al., 2008)) are that water uptake is determined separately  
 353 by the inorganic compounds and organics (i.e., the effect of mixing state was ignored) (Myhre et al., 2007; Nandy et al., 2021),  
 354 thereby our results implied further effect of mixing states on estimations of aerosol hygroscopicity (e.g., growth factor), optical  
 355 properties, and radiative forcing.

356 During dehydration, we investigated phase-separated before and after efflorescence for inorganic salts-organic surfactant

357 particles. Compared with homogeneous particles, phase-separated particles could decrease trace gas uptake (You et al., 2012),  
358 resulting in reduction of the formation of secondary organic aerosols (SOAs) (Zhang et al., 2018). In addition, organic phase  
359 was enriched in “outer shell”, which can potentially alter aerosol water activity and lower aerosol surface tension, hence  
360 affecting aerosol–cloud interactions because water uptake of organic matter in current models (e.g. MPMPO (Griffin et al.,  
361 2003) and SOA treatment in CMAQ v5.2 (Pye et al., 2017)) is estimated by highly parameterized relationships assuming ideal  
362 solutions, e.g., using the kappa hygroscopicity parameter with water surface tension (Petters and Kreidenweis, 2007; Nandy  
363 et al., 2021).

364 Our results provide comprehensive information of mixing states between inorganic salts and organic surfactant in  
365 nanoscale perspective, which could help the establish of incorporation atmospheric modeling, to improve predictions on  
366 indirect effects of aerosol–climate interactions. We should note that in the atmosphere most particles are smaller (e.g., 0.1 to  
367 0.3  $\mu\text{m}$ ) than sample particles and the chemical characteristics of ambient aerosol are not as simple as binary chemical systems  
368 in the current study. Therefore, the water kinetic inhibition should be further investigated for smaller particles containing more  
369 complex systems in the future.

370 Inorganic salts with organic coating are ubiquitous in natural (e.g., marine aerosol) and anthropogenic aerosols (Yu et al.,  
371 2019; Li et al., 2021). Based on the direct observation of mixing state for inorganic surfactants submicron particles, we  
372 confirmed an apparent water diffusion hindrance by organic surfactant shell upon hydration, which could notably raise  
373 inorganic deliquescence RH to nearly saturated condition. This indicates that the hygroscopicity of aerosol would be reduced  
374 in the presence of organic surfactant shell, which might decrease aerosol water content and inhibit aqueous reactions (e.g.,  
375 aqueous sulfate production).

376 During dehydration, inorganic surfactant particles were phase-separated before and after efflorescence. Surfactants with  
377 lower O:C ratio were more likely to undergo LLPS than those with higher O:C. Compared with homogeneous particles,  
378 phase-separated particles could decrease trace gas uptake (You et al., 2012), resulting in reduction of the formation of  
379 secondary organic aerosols (SOAs) (Zhang et al., 2018). In addition, organic phase was enriched in “outer shell”, which can  
380 potentially alter aerosol water activity and lower aerosol surface tension, hence affecting air liquid interfacial chemistry as  
381 well as aerosol–cloud interactions (Ruehl et al., 2016; Ovadnevaite et al., 2017).

382 We should note that in the atmosphere most particles are smaller (e.g., 0.1 to 0.3  $\mu\text{m}$ ) than sample particles and the  
383 chemical characteristics of ambient aerosol are not as simple as binary chemical systems in the current study. Therefore, the  
384 water kinetic inhibition should be further investigated for smaller particles containing more complex systems in the future. In  
385 all, information of mixing states of inorganic surfactants particles should be incorporated into the atmospheric modeling for  
386 heterogeneous chemistry, particle hygroscopicity and growth, to improve predictions on indirect effects of aerosol–climate  
387 interactions.

389 Atmospheric surfactants have potential to distribute to surface, altering mixing state hence influencing aerosol  
390 hygroscopicity and CCN activity. But currently direct observation of RH-depended mixing state of aerosol containing  
391 atmospheric surfactants is scarce. In this study, dynamic mixing state and phase transitions of 20 types of submicron particles  
392 containing inorganic and surface-active organic constituents were directly investigated upon relative humidity (RH) cycling  
393 by Environmental Scanning Electron Microscopy (ESEM).

394 Inorganic-organic core-shell morphology was found for dry deposited mixed inorganic salt-organic surfactant particles.  
395 During hydration, organic shell inhibited water diffusion exposing to inorganic cores, resulting in higher deliquescence RH  
396 (88.3–99.5%) of inner inorganic phase compared with pure inorganic aerosol. This was because higher RH may facilitate phase  
397 transition of organic shell from solid to semisolid, raising organic viscosity thus decreasing water diffusion exposing to  
398 inorganic core. Meanwhile, we directly observed obvious Ostwald ripening of NaCl in single partiele, that is, the growth of  
399 larger NaCl crystal at the expense of smaller ones, in 6 among 10 NaCl-organic surfactants systems. As a result of water  
400 inhibition by surfactant shell, Ostwald ripening in all systems occurred at RH above 90%, which were higher than reported  
401 RH range of pure NaCl measured at 27°C (75–77%).

402 During dehydration, 8 among 20 chemical systems underwent LLPS, including 4 AS-organic surfactant systems and 4  
403 NaCl-organic surfactant systems. LLPS was always observed when O:C  $\leq 0.4$  and never been observed when O:C  $> \sim 0.57$ .  
404 SRH values of AS-organic surfactant particles were generally higher than SRH of corresponding NaCl-organic surfactant  
405 systems, which was consistent with reported salting out efficiency of inorganic salts. OVF showed a controversial effect on  
406 SRH of inorganic salt-organic surfactant systems. Additionally, inorganic salts-organic surfactant systems without LLPS  
407 underwent solid phase separation after efflorescence and also showed distinct separated phases. Our results provide a  
408 comprehensive and unique insights into the dynamic evolution of inorganic salt-organic surfactant particles under fluctuating  
409 atmospheric conditions, which could help improve our fundamental knowledge and decrease uncertainty of model estimation  
410 on global radiative effect.

411

412 **Data availability.** The experiment data are available at ZENODO (<https://doi.org/10.5281/zenodo.8079001>)

413

414 **Author contributions.** CX and BK did the experiments, analyzed data. CX plotted the figures and wrote the original draft. FZ  
415 and XP contributed to discussion and reviewed the manuscript. BK and ZX reviewed the manuscript and contributed to the  
416 fund acquisition. ZW administrated the project, conceptualized the study, reviewed the manuscript and contributed to fund  
417 acquisition.

418

419 **Financial support.** The research was supported by National Natural Science Foundation of China (91844301, 41805100,

420 42005087, and 42005086) and the Key Research and Development Program of Zhejiang Province (2021C03165 and  
421 2022C03084).

422

423 **Acknowledgment.** We thank Yuzhong Zhang from School of Engineering, Lin Liu and Wenjing Cao from Instrumentation and  
424 Service Center for Physical Sciences at Westlake University for the supporting in ESEM experiments.

425

426 **Competing interests.** The authors declare no competing financial interest.

## 427 **Reference**

428 Altaf, M. B. and Freedman, M. A.: Effect of Drying Rate on Aerosol Particle Morphology, *J. Phys. Chem. Lett.*, 8,  
429 3613-3618, <https://doi.org/10.1021/acs.jpcclett.7b01327>, 2017.

430 Altaf, M. B., Dutcher, D. D., Raymond, T. M., and Freedman, M. A.: Effect of Particle Morphology on Cloud  
431 Condensation Nuclei Activity, *ACS Earth Space Chem.*, 2, 634-639,  
432 <https://doi.org/10.1021/acsearthspacechem.7b00146>, 2018.

433 Bertram, A. K., Martin, S. T., Hanna, S. J., Smith, M. L., Bodsworth, A., Chen, Q., Kuwata, M., Liu, A., You, Y.,  
434 and Zorn, S. R.: Predicting the Relative Humidities of Liquid-Liquid Phase Separation, Efflorescence, and  
435 Deliquescence of Mixed Particles of Ammonium Sulfate, Organic Material, and Water Using the Organic-to-  
436 Sulfate Mass Ratio of the Particle and the Oxygen-to-Carbon Elemental Ratio of the Organic Component,  
437 *Atmos. Chem. Phys.*, 11, 10995-11006, <https://doi.org/10.5194/acp-11-10995-2011>, 2011.

438 Boistelle, R. and Astier, J. P.: Crystallization Mechanisms in Solution, *J. Cryst. Growth*, 90, 14-30,  
439 [https://doi.org/10.1016/0022-0248\(88\)90294-1](https://doi.org/10.1016/0022-0248(88)90294-1), 1988.

440 Bruggemann, M., Xu, R. S., Tilgner, A., Kwong, K. C., Mutzel, A., Poon, H. Y., Otto, T., Schaefer, T., Poulain, L.,  
441 Chan, M. N., and Herrmann, H.: Organosulfates in Ambient Aerosol: State of Knowledge and Future Research  
442 Directions on Formation, Abundance, Fate, and Importance, *Environ. Sci. Technol.*, 54, 3767-3782,  
443 <https://doi.org/10.1021/acs.est.9b06751>, 2020.

444 Cheng, M. Q. and Kuwata, M.: Development of the Low-Temperature Hygroscopicity Tandem Differential  
445 Mobility Analyzer (Low-T HTDMA) and its Application to (NH<sub>4</sub>)<sub>2</sub>SO<sub>4</sub> and NaCl Particles, *J. Aerosol Sci.*,  
446 168, 106111, <https://doi.org/10.1016/j.jaerosci.2022.106111>, 2023.

447 Choi, M. Y. and Chan, C. K.: The Effects of Organic Species on the Hygroscopic Behaviors of Inorganic Aerosols,  
448 *Environ. Sci. Technol.*, 36, 2422-2428, <https://doi.org/10.1021/es0113293>, 2002.

- 449 Ciobanu, V. G., Marcolli, C., Krieger, U. K., Weers, U., and Peter, T.: Liquid-Liquid Phase Separation in Mixed  
450 Organic/Inorganic Aerosol Particles, *J. Phys. Chem. A*, 113, 10966-10978, <https://doi.org/10.1021/jp905054d>,  
451 2009.
- 452 Fountoukis, C. and Nenes, A.: ISORROPIA II: a computationally efficient thermodynamic equilibrium model for  
453  $K^+$ - $Ca^{2+}$ - $Mg^{2+}$ - $NH_4^+$ - $Na^+$ - $SO_4^{2-}$ - $NO_3^-$ - $Cl^-$ - $H_2O$  aerosols, *Atmos. Chem. Phys.*, 7, 4639-4659,  
454 <https://doi.org/10.5194/acp-7-4639-2007>, 2007.
- 455 Freedman, M. A.: Liquid-Liquid Phase Separation in Supermicrometer and Submicrometer Aerosol Particles, *Acc.*  
456 *Chem. Res.*, 53, 1102-1110, <https://doi.org/10.1021/acs.accounts.0c00093>, 2020.
- 457 Ghorai, S., Wang, B. B., Tivanski, A., and Laskin, A.: Hygroscopic Properties of Internally Mixed Particles  
458 Composed of NaCl and Water-Soluble Organic Acids, *Environ. Sci. Technol.*, 48, 2234-2241,  
459 <https://doi.org/10.1021/es404727u>, 2014.
- 460 Griffin, R. J., Nguyen, K., Dabdub, D., and Seinfeld, J. H.: A coupled hydrophobic-hydrophilic model for predicting  
461 secondary organic aerosol formation, *J. Atmos. Chem.*, 44, 171-190,  
462 <https://doi.org/10.1023/A:1022436813699>, 2003.
- 463 Guo, L. Y., Peng, C., Zong, T. M., Gu, W. J., Ma, Q. X., Wu, Z. J., Wang, Z., Ding, X., Hu, M., Wang, X. M., and  
464 Tang, M. J.: Comprehensive Characterization of Hygroscopic Properties of Methanesulfonates, *Atmos.*  
465 *Environ.*, 224, 117349, <https://doi.org/10.1016/j.atmosenv.2020.117349>, 2020.
- 466 Ho, K. F., Lee, S. C., Ho, S. S. H., Kawamura, K., Tachibana, E., Cheng, Y., and Zhu, T.: Dicarboxylic acids,  
467 ketocarboxylic acids,  $\alpha$ -dicarbonyls, fatty acids, and benzoic acid in urban aerosols collected during the 2006  
468 Campaign of Air Quality Research in Beijing (CAREBeijing-2006), *J. Geophys. Res.: Atmos.*, 115, D19312,  
469 <https://doi.org/10.1029/2009jd013304>, 2010.
- 470 Hyder, M., Genberg, J., Sandahl, M., Swietlicki, E., and Jönsson, J. Å.: Yearly trend of dicarboxylic acids in organic  
471 aerosols from south of Sweden and source attribution, *Atmos. Environ.*, 57, 197-204,  
472 <https://doi.org/10.1016/j.atmosenv.2012.04.027>, 2012.
- 473 Kirpes, R. M., Lei, Z. Y., Fraund, M., Gansch, M. J., May, N. W., Barrett, T. E., Moffett, C. E., Schauer, A. J.,  
474 Alexander, B., Upchurch, L. M., China, S., Quinn, P. K., Moffet, R. C., Laskin, A., Sheesley, R. J., Pratt, K.  
475 A., and Ault, A. P.: Solid organic-coated ammonium sulfate particles at high relative humidity in the  
476 summertime Arctic atmosphere, *Proc. Natl. Acad. Sci. U.S.A.*, 119, <https://doi.org/10.1073/pnas.2104496119>,  
477 2022.
- 478 Kwamena, N. O. A., Buajareern, J., and Reid, J. P.: Equilibrium Morphology of Mixed Organic/Inorganic/Aqueous

479 Aerosol Droplets: Investigating the Effect of Relative Humidity and Surfactants, *J. Phys. Chem. A*, 114, 5787-  
480 5795, <https://doi.org/10.1021/jp1003648>, 2010.

481 Lambert, F., Kug, J. S., Park, R. J., Mahowald, N., Winckler, G., Abe-Ouchi, A., O'ishi, R., Takemura, T., and Lee,  
482 J. H.: The role of mineral-dust aerosols in polar temperature amplification, *Nat. Clim. Change*, 3, 487-491,  
483 <https://doi.org/10.1038/Nclimate1785>, 2013.

484 Laskin, A., Cowin, J. P., and Iedema, M. J.: Analysis of Individual Environmental Particles using Modern Methods  
485 of Electron Microscopy and X-ray Microanalysis, *J. Electron. Spectrosc. Relat. Phenom.*, 150, 260-274,  
486 <https://doi.org/10.1016/j.elspec.2005.06.008>, 2006.

487 Laskina, O., Morris, H. S., Grandquist, J. R., Qiu, Z., Stone, E. A., Tivanski, A. V., and Grassian, V. H.: Size Matters  
488 in the Water Uptake and Hygroscopic Growth of Atmospherically Relevant Multicomponent Aerosol Particles,  
489 *J. Phys. Chem. A*, 119, 4489-4497, <https://doi.org/10.1021/jp510268p>, 2015.

490 Li, W. J., Shao, L. Y., Zhang, D. Z., Ro, C. U., Hu, M., Bi, X. H., Geng, H., Matsuki, A., Niu, H. Y., and Chen, J.  
491 M.: A review of single aerosol particle studies in the atmosphere of East Asia: morphology, mixing state,  
492 source, and heterogeneous reactions, *J. Cleaner Prod.*, 112, 1330-1349,  
493 <https://doi.org/10.1016/j.jclepro.2015.04.050>, 2016.

494 Li, W. J., Teng, X. M., Chen, X. Y., Liu, L., Xu, L., Zhang, J., Wang, Y. Y., Zhang, Y., and Shi, Z. B.: Organic  
495 Coating Reduces Hygroscopic Growth of Phase-Separated Aerosol Particles, *Environ. Sci. Technol.*, 55,  
496 16339-16346, <https://doi.org/10.1021/acs.est.1c05901>, 2021.

497 Ma, S. S., Pang, S. F., Li, J., and Zhang, Y. H.: A review of efflorescence kinetics studies on atmospherically relevant  
498 particles, *Chemosphere*, 277, 130320, <https://doi.org/10.1016/j.chemosphere.2021.130320>, 2021.

499 Martin, S. T.: Phase Transitions of Aqueous Atmospheric Particles, *Chem. Rev.*, 100, 3403-3453,  
500 <https://doi.org/10.1021/cr990034t>, 2000.

501 Metzger, S., Dentener, F., Krol, M., Jeuken, A., and Lelieveld, J.: Gas/aerosol partitioning 2. Global modeling  
502 results, *Journal of Geophysical Research-Atmospheres*, 107, ACH-17, <https://doi.org/10.1029/2001jd001103>,  
503 2002a.

504 Metzger, S., Dentener, F., Pandis, S., and Lelieveld, J.: Gas/aerosol partitioning 1. A computationally efficient  
505 model, *Journal of Geophysical Research-Atmospheres*, 107, D16, <https://doi.org/10.1029/2001jd001102>,  
506 2002b.

507 Myhre, G., Bellouin, N., Berglen, T. F., Berntsen, T. K., Boucher, O., Grini, A., Isaksen, I. S. A., Johnsrud, M.,  
508 Mishchenko, M. I., Stordal, F., and Tanre, D.: Comparison of the radiative properties and direct radiative effect

509 of aerosols from a global aerosol model and remote sensing data over ocean, *Tellus B*, 59, 115-129,  
510 <https://doi.org/10.1111/j.1600-0889.2006.00238.x>, 2007.

511 Nandy, L., Yao, Y., Zheng, Z. H., and Riemer, N.: Water uptake and optical properties of mixed organic-inorganic  
512 particles, *Aerosol Sci. Technol.*, 55, 1398-1413, <https://doi.org/10.1080/02786826.2021.1966378>, 2021.

513 Nguyen, Q. T., Kjær, K. H., Kling, K. I., Boesen, T., and Bilde, M.: Impact of Fatty Acid Coating on the CCN  
514 Activity of Sea Salt Particles, *Tellus B: Chem. Phys. Meteorol.*, 69, 1304064,  
515 <https://doi.org/10.1080/16000889.2017.1304064>, 2017.

516 Noziere, B.: Don't Forget the Surface, *Science*, 351, 1396-1397, <https://doi.org/10.1126/science.aaf3253>, 2016.

517 O'Brien, R. E., Wang, B. B., Kelly, S. T., Lundt, N., You, Y., Bertram, A. K., Leone, S. R., Laskin, A., and Gilles,  
518 M. K.: Liquid-Liquid Phase Separation in Aerosol Particles: Imaging at the Nanometer Scale, *Environ. Sci.*  
519 *Technol.*, 49, 4995-5002, <https://doi.org/10.1021/acs.est.5b00062>, 2015.

520 Ohno, P. E., Qin, Y. M., Ye, J. H., Wang, J. F., Bertram, A. K., and Martin, S. T.: Fluorescence Aerosol Flow Tube  
521 Spectroscopy to Detect Liquid-Liquid Phase Separation, *ACS Earth Space Chem.*, 5, 1223-1232,  
522 <https://doi.org/10.1021/acsearthspacechem.1c00061>, 2021.

523 Ohno, P. E., Brandao, L., Rainone, E. M., Aruffo, E., Wang, J. F., Qin, Y. M., and Martin, S. T.: Size Dependence  
524 of Liquid-Liquid Phase Separation by in Situ Study of Flowing Submicron Aerosol Particles, *J. Phys. Chem.*  
525 *A*, 127, 2967-2974, <https://doi.org/10.1021/acs.jpca.2c08224>, 2023.

526 Onasch, T. B., Siefert, R. L., Brooks, S. D., Prenni, A. J., Murray, B., Wilson, M. A., and Tolbert, M. A.: Infrared  
527 Spectroscopic Study of The Deliquescence and Efflorescence of Ammonium Sulfate Aerosol as a Function of  
528 Temperature, *Journal of Geophysical Research-Atmospheres*, 104, 21317-21326,  
529 <https://doi.org/10.1029/1999jd900384>, 1999.

530 Ott, E. J. E. and Freedman, M. A.: Influence of Ions on the Size Dependent Morphology of Aerosol Particles, *ACS*  
531 *Earth Space Chem.*, 5, 2320-2328, <https://doi.org/10.1021/acsearthspacechem.1c00210>, 2021.

532 Ott, E. J. E., Kucinski, T. M., Dawson, J. N., and Freedman, M. A.: Use of Transmission Electron Microscopy for  
533 Analysis of Aerosol Particles and Strategies for Imaging Fragile Particles, *Anal. Chem.*, 93, 11347-11356,  
534 <https://doi.org/10.1021/acs.analchem.0c05225>, 2021.

535 Peng, C., Chan, M. N., and Chan, C. K.: The Hygroscopic Properties of Dicarboxylic and Multifunctional Acids:  
536 Measurements and UNIFAC Predictions, *Environ. Sci. Technol.*, 35, 4495-4501,  
537 <https://doi.org/10.1021/es0107531>, 2001.

538 Peng, C., Jing, B., Guo, Y. C., Zhang, Y. H., and Ge, M. F.: Hygroscopic Behavior of Multicomponent Aerosols



539 Involving NaCl and Dicarboxylic Acids, *J. Phys. Chem. A*, 120, 1029-1038,  
540 <https://doi.org/10.1021/acs.jpca.5b09373>, 2016.

541 Peng, C., Chen, L., and Tang, M.: A Database for Deliquescence and Efflorescence Relative Humidities of  
542 Compounds with Atmospheric Relevance, *Fundam. Res.*, 2, 578-587,  
543 <https://doi.org/10.1016/j.fmre.2021.11.021>, 2022.

544 Petters, M. D. and Kreidenweis, S. M.: A single parameter representation of hygroscopic growth and cloud  
545 condensation nucleus activity, *Atmos. Chem. Phys.*, 7, 1961-1971, <https://doi.org/10.5194/acp-7-1961-2007>,  
546 2007.

547 Pöhlker, C., Saturno, J., Krüger, M. L., Förster, J. D., Weigand, M., Wiedemann, K. T., Bechtel, M., Artaxo, P., and  
548 Andreae, M. O.: Efflorescence upon Humidification? X-ray Microspectroscopic in situ Observation of  
549 Changes in Aerosol Microstructure and Phase State upon Hydration, *Geophys. Res. Lett.*, 41, 3681-3689,  
550 <https://doi.org/10.1002/2014gl059409>, 2014.

551 Pöschl, U.: Atmospheric Aerosols: Composition, Transformation, Climate and Health Effects, *Angew. Chem. Int.*  
552 *Ed.*, 44, 7520-7540, <https://doi.org/10.1002/anie.200501122>, 2005.

553 Posfai, M., Axisa, D., Tompa, E., Freney, E., Bruinjes, R., and Buseck, P. R.: Interactions of Mineral Dust with  
554 Pollution and Clouds: An Individual-Particle TEM Study of Atmospheric Aerosol from Saudi Arabia, *Atmos.*  
555 *Res.*, 122, 347-361, <https://doi.org/10.1016/j.atmosres.2012.12.001>, 2013.

556 Pye, H. O. T., Murphy, B. N., Xu, L., Ng, N. L., Carlton, A. G., Guo, H. Y., Weber, R., Vasilakos, P., Appel, K. W.,  
557 Budisulistiorini, S. H., Surratt, J. D., Nenes, A., Hu, W. W., Jimenez, J. L., Isaacman-VanWertz, G., Misztal,  
558 P. K., and Goldstein, A. H.: On the implications of aerosol liquid water and phase separation for organic aerosol  
559 mass, *Atmos. Chem. Phys.*, 17, 343-369, <https://doi.org/10.5194/acp-17-343-2017>, 2017.

560 Reed, N. W., Wing, B. A., Tolbert, M. A., and Browne, E. C.: Trace H<sub>2</sub>S Promotes Organic Aerosol Production and  
561 Organosulfur Compound Formation in Archean Analog Haze Photochemistry Experiments, *Geophys. Res.*  
562 *Lett.*, 49, <https://doi.org/10.1029/2021GL097032>, 2022.

563 Riemer, N., Ault, A. P., West, M., Craig, R. L., and Curtis, J. H.: Aerosol Mixing State: Measurements, Modeling,  
564 and Impacts, *Rev. Geophys.*, 57, 187-249, <https://doi.org/10.1029/2018rg000615>, 2019.

565 Römpp, A., Winterhalter, R., and Moortgat, G. K.: Oxodicarboxylic acids in atmospheric aerosol particles, *Atmos.*  
566 *Environ.*, 40, 6846-6862, <https://doi.org/10.1016/j.atmosenv.2006.05.053>, 2006.

567 Roy, P., Mael, L. E., Makhnenko, I., Martz, R., Grassian, V. H., and Dutcher, C. S.: Temperature-Dependent Phase  
568 Transitions of Aqueous Aerosol Droplet Systems in Microfluidic Traps, *ACS Earth Space Chem.*, 4, 1527-

569 1539, <https://doi.org/10.1021/acsearthspacechem.0c00114>, 2020.

570 Ruehl, C. R. and Wilson, K. R.: Surface Organic Monolayers Control the Hygroscopic Growth of Submicrometer  
571 Particles at High Relative Humidity, *J. Phys. Chem. A*, 118, 3952-3966, <https://doi.org/10.1021/jp502844g>,  
572 2014.

573 Ruehl, C. R., Davies, J. F., and Wilson, K. R.: An Interfacial Mechanism for Cloud Droplet Formation on Organic  
574 Aerosols, *Science*, 351, 1447-1450, <https://doi.org/10.1126/science.aad4889>, 2016.

575 Shiraiwa, M., Zuend, A., Bertram, A. K., and Seinfeld, J. H.: Gas-Particle Partitioning of Atmospheric Aerosols:  
576 Interplay of Physical State, Non-Ideal Mixing and Morphology, *Physical Chemistry Chemical Physics*, 15,  
577 11441-11453, <https://doi.org/10.1039/c3cp51595h>, 2013.

578 Song, M., Marcolli, C., Krieger, U. K., Zuend, A., and Peter, T.: Liquid-Liquid Phase Separation and Morphology  
579 of Internally Mixed Dicarboxylic Acids/Ammonium Sulfate/Water Particles, *Atmos. Chem. Phys.*, 12, 2691-  
580 2712, <https://doi.org/10.5194/acp-12-2691-2012>, 2012a.

581 Song, M., Marcolli, C., Krieger, U. K., Zuend, A., and Peter, T.: Liquid-Liquid Phase Separation in Aerosol Particles:  
582 Dependence on O:C, Organic Functionalities, and Compositional Complexity, *Geophys. Res. Lett.*, 39,  
583 L19801, <https://doi.org/10.1029/2012gl052807>, 2012b.

584 Song, M., Maclean, A. M., Huang, Y. Z., Smith, N. R., Blair, S. L., Laskin, J., Laskin, A., DeRieux, W. S. W., Li,  
585 Y., Shiraiwa, M., Nizkorodov, S. A., and Bertram, A. K.: Liquid-Liquid Phase Separation and Viscosity within  
586 Secondary Organic Aerosol Generated from Diesel Fuel Vapors, *Atmos. Chem. Phys.*, 19, 12515-12529,  
587 <https://doi.org/10.5194/acp-19-12515-2019>, 2019.

588 Song, M. J., Liu, P. F., Martin, S. T., and Bertram, A. K.: Liquid-Liquid Phase Separation in Particles Containing  
589 Secondary Organic Material Free of Inorganic Salts, *Atmos. Chem. Phys.*, 17, 11261-11271,  
590 <https://doi.org/10.5194/acp-17-11261-2017>, 2017.

591 Stewart, D. J., Cai, C., Naylor, J., Preston, T. C., Reid, J. P., Krieger, U. K., Marcolli, C., and Zhang, Y. H.: Liquid-  
592 Liquid Phase Separation in Mixed Organic/Inorganic Single Aqueous Aerosol Droplets, *J. Phys. Chem. A*, 119,  
593 4177-4190, <https://doi.org/10.1021/acs.jpca.5b01658>, 2015.

594 Takahama, S., Pathak, R. K., and Pandis, S. N.: Efflorescence Transitions of Ammonium Sulfate Particles Coated  
595 with Secondary Organic Aerosol, *Environ. Sci. Technol.*, 41, 2289-2295, <https://doi.org/10.1021/es0619915>,  
596 2007.

597 Ting, Y. C., Mitchell, E. J. S., Allan, J. D., Liu, D. T., Spracklen, D. V., Williams, A., Jones, J. M., Lea-Langton, A.  
598 R., McFiggans, G., and Coe, H.: Mixing State of Carbonaceous Aerosols of Primary Emissions from

599 "Improved" African Cookstoves, *Environ. Sci. Technol.*, 52, 10134-10143,  
600 <https://doi.org/10.1021/acs.est.8b00456>, 2018.

601 Tolocka, M. P. and Turpin, B.: Contribution of Organosulfur Compounds to Organic Aerosol Mass, *Environ. Sci.*  
602 *Technol.*, 46, 7978-7983, <https://doi.org/10.1021/es300651v>, 2012.

603 Tong, Y. K., Meng, X. X. Y., Zhou, B., Sun, R., Wu, Z. J., Hu, M., and Ye, A. P.: Detecting the pH-dependent liquid-  
604 liquid phase separation of single levitated aerosol microdroplets via laser tweezers-Raman spectroscopy, *Front.*  
605 *Phys.*, 10, <https://doi.org/10.3389/fphy.2022.969921>, 2022.

606 Unga, F., Choel, M., Derimian, Y., Deboudt, K., Dubovik, O., and Goloub, P.: Microscopic Observations of Core-  
607 Shell Particle Structure and Implications for Atmospheric Aerosol Remote Sensing, *Journal of Geophysical*  
608 *Research-Atmospheres*, 123, 13944-13962, <https://doi.org/10.1029/2018jd028602>, 2018.

609 Veghte, D. P., Bittner, D. R., and Freedman, M. A.: Cryo-Transmission Electron Microscopy Imaging of the  
610 Morphology of Submicrometer Aerosol Containing Organic Acids and Ammonium Sulfate, *Anal. Chem.*, 86,  
611 2436-2442, <https://doi.org/10.1021/ac403279f>, 2014.

612 Voorhees, P. W.: The Theory of Ostwald Ripening, *J. Stat. Phys.*, 38, 231-252, <https://doi.org/10.1007/Bf01017860>,  
613 1985.

614 Wang, N., Jing, B., Wang, P., Wang, Z., Li, J. R., Pang, S. F., Zhang, Y. H., and Ge, M. F.: Hygroscopicity and  
615 Compositional Evolution of Atmospheric Aerosols Containing Water-Soluble Carboxylic Acid Salts and  
616 Ammonium Sulfate: Influence of Ammonium Depletion, *Environ. Sci. Technol.*, 53, 6225-6234,  
617 <https://doi.org/10.1021/acs.est.8b07052>, 2019.

618 Wang, W. H., Shao, L. Y., Mazzoleni, C., Li, Y. W., Kotthaus, S., Grimmond, S., Bhandari, J., Xing, J. P., Feng, X.  
619 L., Zhang, M. Y., and Shi, Z. B.: Measurement report: Comparison of wintertime individual particles at ground  
620 level and above the mixed layer in urban Beijing, *Atmos. Chem. Phys.*, 21, 5301-5314,  
621 <https://doi.org/10.5194/acp-21-5301-2021>, 2021.

622 Wise, M. E., Martin, S. T., Russell, L. M., and Buseck, P. R.: Water Uptake by NaCl Particles Prior to Deliquescence  
623 and the Phase Rule, *Aerosol Sci. Technol.*, 42, 281-294, <https://doi.org/10.1080/02786820802047115>, 2008.

624 Xiong, C., Chen, X. Y., Ding, X. L., Kuang, B. Y., Pei, X. Y., Xu, Z. N., Yang, S. K., Hu, H., and Wang, Z. B.:  
625 Reconsideration of Surface Tension and Phase State Effects on Cloud Condensation Nuclei Activity Based on  
626 the Atomic Force Microscopy Measurement, *Atmos. Chem. Phys.*, 22, 16123-16135,  
627 <https://doi.org/10.5194/acp-22-16123-2022>, 2022.

628 Xu, L., Fukushima, S., Sobanska, S., Murata, K., Naganuma, A., Liu, L., Wang, Y. Y., Niu, H. Y., Shi, Z. B., Kojima,

629 T., Zhang, D. Z., and Li, W. J.: Tracing the evolution of morphology and mixing state of soot particles along  
630 with the movement of an Asian dust storm, *Atmos. Chem. Phys.*, 20, 14321-14332,  
631 <https://doi.org/10.5194/acp-20-14321-2020>, 2020.

632 Xu, W. Q., Chen, C., Qiu, Y. M., Li, Y., Zhang, Z. Q., Karnezi, E., Pandis, S. N., Xie, C. H., Li, Z. J., Sun, J. X.,  
633 Ma, N., Xu, W. Y., Fu, P. Q., Wang, Z. F., Zhu, J., Worsnop, D. R., Ng, N. L., and Sun, Y. L.: Organic aerosol  
634 volatility and viscosity in the North China Plain: contrast between summer and winter, *Atmos. Chem. Phys.*,  
635 21, 5463-5476, <https://doi.org/10.5194/acp-21-5463-2021>, 2021.

636 Yang, H., Wang, N., Pang, S. F., Zheng, C. M., and Zhang, Y. H.: Chemical reaction between sodium pyruvate and  
637 ammonium sulfate in aerosol particles and resultant sodium sulfate efflorescence, *Chemosphere*, 215, 554-  
638 562, <https://doi.org/10.1016/j.chemosphere.2018.10.062>, 2019.

639 You, Y., Renbaum-Wolff, L., Carreras-Sospedra, M., Hanna, S. J., Hiranuma, N., Kamal, S., Smith, M. L., Zhang,  
640 X. L., Weber, R. J., Shilling, J. E., Dabdub, D., Martin, S. T., and Bertram, A. K.: Images Reveal that  
641 Atmospheric Particles can Undergo Liquid-Liquid Phase Separations, *Proc. Natl. Acad. Sci. U.S.A.*, 109,  
642 13188-13193, <https://doi.org/10.1073/pnas.1206414109>, 2012.

643 You, Y., Renbaum-Wolff, L., and Bertram, A. K.: Liquid-liquid phase separation in particles containing organics  
644 mixed with ammonium sulfate, ammonium bisulfate, ammonium nitrate or sodium chloride, *Atmos. Chem.*  
645 *Phys.*, 13, 11723-11734, <https://doi.org/10.5194/acp-13-11723-2013>, 2013.

646 You, Y. and Bertram, A. K.: Effects of Molecular Weight and Temperature on Liquid-Liquid Phase Separation in  
647 Particles Containing Organic Species and Inorganic Salts, *Atmos. Chem. Phys.*, 15, 1351-1365,  
648 <https://doi.org/10.5194/acp-15-1351-2015>, 2015.

649 Zavacka, K., Nedela, V., Olbert, M., Tihlarikova, E., Vetrakova, L., Yang, X., and Heger, D.: Temperature and  
650 Concentration Affect Particle Size Upon Sublimation of Saline Ice: Implications for Sea Salt Aerosol  
651 Production in Polar Regions, *Geophys. Res. Lett.*, 49, <https://doi.org/10.1029/2021GL097098>, 2022.

652 Zaveri, R. A., Easter, R. C., Fast, J. D., and Peters, L. K.: Model for Simulating Aerosol Interactions and Chemistry  
653 (MOSAIC), *Journal of Geophysical Research-Atmospheres*, 113, D13204,  
654 <https://doi.org/10.1029/2007jd008782>, 2008.

655 Zeng, G., Kelley, J., Kish, J. D., and Liu, Y.: Temperature-Dependent Deliquescent and Efflorescent Properties of  
656 Methanesulfonate Sodium Studied by ATR-FTIR Spectroscopy, *J. Phys. Chem. A*, 118, 583-591,  
657 <https://doi.org/10.1021/jp405896y>, 2014.

658 Zhang, J., Yuan, Q., Liu, L., Wang, Y. Y., Zhang, Y. X., Xu, L., Pang, Y., Zhu, Y. H., Niu, H. Y., Shao, L. Y., Yang,

659 S. S., Liu, H., Pan, X. L., Shi, Z. B., Hu, M., Fu, P. Q., and Li, W. J.: Trans-Regional Transport of Haze  
660 Particles From the North China Plain to Yangtze River Delta During Winter, *Journal of Geophysical Research-*  
661 *Atmospheres*, 126, <https://doi.org/10.1029/2020JD033778>, 2021.

662 Zhang, J., Wang, Y. Y., Teng, X. M., Liu, L., Xu, Y. S., Ren, L. H., Shi, Z. B., Zhang, Y., Jiang, J. K., Liu, D. T., Hu,  
663 M., Shao, L. Y., Chen, J. M., Martin, S. T., Zhang, X. Y., and Li, W. J.: Liquid-Liquid Phase Separation Reduces  
664 Radiative Absorption by Aged Black Carbon Aerosols, *Commun. Earth Environ.*, 3, 128,  
665 <https://doi.org/10.1038/s43247-022-00462-1>, 2022.

666 Zhang, Y., Chen, Y. Z., Lambe, A. T., Olson, N. E., Lei, Z. Y., Craig, R. L., Zhang, Z. F., Gold, A., Onasch, T. B.,  
667 Jayne, J. T., Worsnop, D. R., Gaston, C. J., Thornton, J. A., Vizuete, W., Ault, A. P., and Surratt, J. D.: Effect  
668 of the Aerosol-Phase State on Secondary Organic Aerosol Formation from the Reactive Uptake of Isoprene-  
669 Derived Epoxydiols (IEPDX), *Environ. Sci. Technol. Lett.*, 5, 167-174,  
670 <https://doi.org/10.1021/acs.estlett.8b00044>, 2018.

671 Zhang, Y. X., Zhang, Q., Yao, Z. L., and Li, H. Y.: Particle Size and Mixing State of Freshly Emitted Black Carbon  
672 from Different Combustion Sources in China, *Environ. Sci. Technol.*, 54, 7766-7774,  
673 <https://doi.org/10.1021/acs.est.9b07373>, 2020.

674 Zhu, Y., Pang, S., and Zhang, Y.: Observations on the unique phase transitions of inorganics relevant due to gluconic  
675 acid in particles, *Atmos. Environ.*, 288, 119313, <https://doi.org/10.1016/j.atmosenv.2022.119313>, 2022.

676